J Neurophysiol 93: 1266–1277, 2005.
First published October 13, 2004; doi:10.1152/jn.00815.2004.

Spatiotemporal Tuning of Optic Flow Inputs to the Vestibulocerebellum in Pigeons: Differences Between Mossy and Climbing Fiber Pathways

Ian R. Winship,[1] Peter L. Hurd,[1] and Douglas R. W. Wylie[1,2]
[1]*Department of Psychology,* [2]*Centre for Neuroscience, University of Alberta, Edmonton, Alberta, Canada*

Submitted 11 August 2004; accepted in final form 8 October 2004

Winship, Ian R., Peter L. Hurd, and Douglas R. W. Wylie. Spatiotemporal tuning of optic flow inputs to the vestibulocerebellum in pigeons: differences between mossy and climbing fiber pathways. *J Neurophysiol* 93: 1266–1277, 2005. First published October 13, 2004; doi:10.1152/jn.00815.2004. The pretectum, accessory optic system (AOS), and vestibulocerebellum (VbC) have been implicated in the analysis of optic flow and generation of the optokinetic response. Recently, using drifting sine-wave gratings as stimuli, it has been shown that pretectal and AOS neurons exhibit spatiotemporal tuning. In this respect, there are two groups: *fast* neurons, which prefer low spatial frequency (SF) and high temporal frequency (TF) gratings, and *slow* neurons, which prefer high SF–low TF gratings. In pigeons, there are two pathways from the pretectum and AOS to the VbC: a climbing fiber (CF) pathway to Purkinje cells (P cells) via the inferior olive and a direct mossy fiber (MF) pathway to the granular layer (GL). In the present study, we assessed spatiotemporal tuning in the VbC of ketamine-anesthetized pigeons using standard extracellular techniques. Recordings were made from 17 optic-flow-sensitive units in the GL, presumably granule cells or MF rosettes, and the complex spike activity (CSA) of 39 P-cells, which reflects CF input. Based on spatiotemporal tuning to gratings moving in the preferred direction, eight GL units were classified as *fast* units, with a primary response to low SF–high TF gratings (mean = 0.13 cpd/8.24 Hz), whereas nine were *slow* units preferring high SF–low TF gratings (mean = 0.68 cpd/0.30 Hz). CSA was almost exclusively tuned to *slow* gratings (mean = 0.67 cpd/0.35 Hz). We conclude that MF input to the VbC is from both *fast* and *slow* cells in the AOS and pretectum, whereas the CF input is primarily tuned to *slow* gratings.

INTRODUCTION

Self-motion through an environment consisting of stationary objects and surfaces results in distinct patterns of visual motion across the entire retina. These characteristic patterns are referred to as "optic flow" or "flowfields" (Gibson 1954). The analysis of optic flow is important for the generation of optokinetic responses, such as optokinetic nystagmus and the optocollic reflex, which facilitate gaze stabilization (for review, see Ilg 1997; see also Carpenter 1988; Robinson 1981; birds, Gioanni 1988; Gioanni et al. 1981, 1983a,b). Gaze stabilization is important to prevent the degradation of visual acuity (Westheimer and McKee 1975) and enhance velocity discrimination (Nakayama 1981).

Numerous studies, using micro-stimulation, lesion, and electrophysiological methods, have implicated nuclei in the accessory optic system (AOS) and pretectum in the analysis of optic flow and the generation of optokinetic responses (for reviews, see Grasse and Cynader 1990; Simpson 1984; Simpson et al. 1988). The AOS and pretectum are highly conserved, and homologous structures have been identified in mammalian and avian species (Fite 1985; McKenna and Wallman 1985; Weber 1985). The mammalian AOS consists of the medial, lateral, and dorsal terminal nuclei (MTN, LTN, and DTN, respectively), which are equivalent to the nucleus of the basal optic root (nBOR) in birds. Likewise the pretectal nucleus of the optic tract (NOT) of mammals is equivalent to the avian pretectal nucleus lentiformis mesencephali (LM) (for reviews, see Simpson 1984; Simpson et al. 1988).

Physiological recordings from the AOS and pretectum from numerous species have shown that neurons in these nuclei have large, contralateral receptive fields and exhibit direction-selectivity to large-field moving stimuli rich in visual texture (NOT: Collewijn 1975a,b; Distler and Hoffmann 1993; Hoffmann and Distler 1989; Hoffman and Schoppmann 1975, 1981; Hoffmann et al. 1988; Ilg and Hoffmann 1996; Klauer et al. 1990; Mustari and Fuchs 1990; Volchan et al. 1989; Yakushin et al. 2000; LM: Fan et al. 1995; Fite et al. 1989; Katte and Hoffmann 1980; McKenna and Wallman 1981, 1985; Winterson and Brauth 1985; Wylie and Frost 1996; MTN/LTN: Grasse and Cynader 1982; Grasse et al. 1984; Simpson et al. 1979; Soodak and Simpson 1988; nBOR, Ariel and Kogo 2001; Burns and Wallman 1981; Gioanni et al. 1984; Kogo et al. 1998, 2002; Morgan and Frost 1981; Rosenberg and Ariel 1990; Wylie and Frost 1990). Recent neurophysiological studies that used large-field sinusoidal gratings as stimuli showed that pretectal and AOS neurons show spatiotemporal tuning. This was first shown in the wallaby NOT (Ibbotson et al. 1994) and subsequently in the pigeon nBOR and LM (Crowder and Wylie 2001; Crowder et al. 2003a,b; Wolf-Oberhollenzer and Kirschfeld 1994; Wylie and Crowder 2000). These studies found that pretectal and AOS neurons fall into two groups based on the location of the peak (maximal) response in the spatiotemporal domain: *slow* cells were maximally sensitive to motion at low temporal frequency (TF $<$ 1 Hz) and high spatial frequency (SF $>$ 0.25 cycles/°, cpd), whereas *fast* cells were maximally sensitive to high TF ($>$1 Hz) and low SF ($<$0.25 cpd) sine wave gratings. Figure 1*A* depicts the fast and slow regions in the spatiotemporal domain. Ibbotson and Price (2001) noted that the spatiotemporal preferences of the *fast* and *slow* units in the pretectum of wallabies and pigeons were remarkably similar. We must caution that the *fast/slow* distinction is not so simplistic. It is not uncommon for a *slow* neuron to show a secondary peak in the *fast* region or a *fast* neuron to show a secondary peak in the *slow* region (Crowder and Wylie

Address for reprint requests and other correspondence: D. R. Wong-Wylie, Dept. of Psychology, University of Alberta, Edmonton, Alberta, Canada T6G 2E9 (E-mail: dwylie@ualberta.ca).

The costs of publication of this article were defrayed in part by the payment of page charges. The article must therefore be hereby marked "*advertisement*" in accordance with 18 U.S.C. Section 1734 solely to indicate this fact.

 0022-3077/05 $8.00 Copyright © 2005 The American Physiological Society

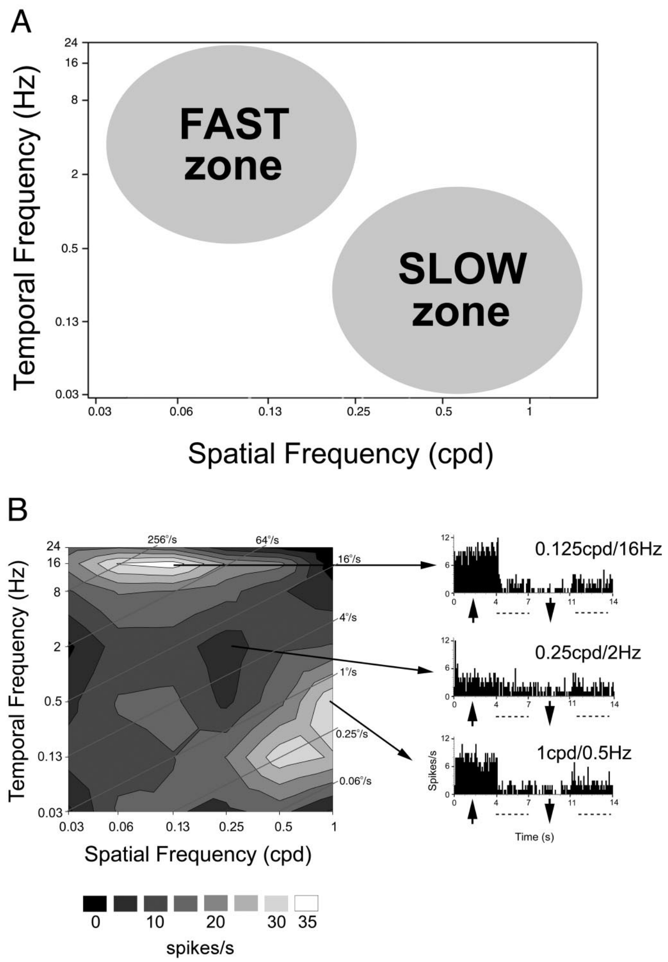

FIG. 1. Spatiotemporal tuning in the accessory optic system (AOS), pretectum, and vestibulocerebellum (VbC). In *A,* the approximate spatiotemporal preferences for *fast* and *slow* neurons in the mammalian and avian AOS and pretectum are illustrated (Crowder and Wylie 2001; Crowder et al. 2003a,b; Ibbotson et al. 1994; Wolf-Oberhollenzer and Kirschfeld 1994; Wylie and Crowder 2000). *B*: the contour plot and peristimulus time histograms (PSTHs) of spatiotemporal tuning for a granular layer (GL) unit in the VbC. The contour plot shows the firing rate in response to sine wave gratings of varying spatial (abscissa) and temporal (ordinate) frequencies drifting in the preferred direction for the unit. The plot is shaded such that white represents the spatial frequency (SF) and temporal frequency (SF–TF) combinations resulting in maximal excitation and black indicates minimal excitation. This unit was spatiotemporally tuned with primary peak in the *fast* zone and a slightly lesser peak in the *slow* zone. PSTHs on the right show the unit's modulation during stimulation in the preferred (upward) and antipreferred (downward) direction for gratings of 3 different SF–TF combinations during a single sweep. The top, middle, and bottom PSTHs show the unit's response to gratings of 0.125 cpd/16 Hz, 0.25 cpd/2 Hz, and 1 cpd/0.5 Hz, respectively. Firing rate is indicated by spikes per second (spikes/s) on the *y* axis and time in seconds is shown on the *x* axis. Gray diagonal lines overlaying the contour plot indicate particular velocities (TF/SF) from 0.06 to 256°/s. See text for additional details.

2001; Crowder et al. 2003a; Ibbotson et al. 1994; Wylie and Crowder 2000). Such neurons likely receive inputs from *fast* and *slow* subunits.

The AOS and pretectum provide input to the optic-flow-sensitive neurons in the vestibulocerebellum (VbC) (for reviews, see Simpson 1984; Simpson et al. 1988; birds, Brecha et al. 1980; Clarke 1977). In birds, there are two inputs from the LM and nBOR to the VbC: an indirect climbing fiber (CF) pathway through the medial column of the inferior olive (mcIO) (Arends and Voogd 1989; Brecha et al. 1980; Clarke 1977; Gamlin and Cohen 1988; Lau et al. 1998; Wylie et al. 1999; Crowder et al. 2000; Winship and Wylie 2001, 2003; Wylie 2001) and a direct mossy fiber (MF) pathway that is mainly restricted to folium IXcd (Brecha and Karten 1979; Brecha et al. 1980; Brauth and Karten 1977; Clarke 1977; Gamlin and Cohen 1988; Wylie and Linkenhoker 1996; Wylie et al. 1997). The CF pathway to the VbC exists in mammals (for reviews, see Simpson 1984; Simpson et al. 1988). The complex spike activity (CSA) of VbC Purkinje cells, which reflects CF input (Thach 1967), is direction selective for particular patterns of optic flow (Graf et al. 1988; Kano et al. 1990; Kusonoki et al. 1990; Simpson et al. 1981; Wylie and Frost 1993, 1999; Wylie et al. 1998). The MF pathway has also been reported in turtles and fish (Fan et al. 1993; Finger and Karten 1978; Reiner and Karten 1978) but not in several mammalian species (Blanks et al. 1983; Giolli et al. 1984; Kawasaki and Sato 1980). Winfield et al. (1978) reported a direct MF pathway from the MTN to the VbC in the chinchilla, although this finding has been contested (Giolli et al. 1984). In this study, in effort to determine whether the *fast* or *slow* cells in the AOS and pretectum feed the MF and CF pathways to the VbC, we recorded the responses of units in the granular layer of folium IXcd and the CSA of VbC Purkinje cells to sine wave gratings of varying TF and SF.

METHODS

Surgery and extracellular recording

The methods reported herein conform to the guidelines established by the Canadian Council on Animal Care and approved by the Biosciences Animal Care and Policy Committee at the University of Alberta. Silver King pigeons (obtained from a local supplier) were anesthetized using an intramuscular ketamine (65 mg/kg) and xylazine (8 mg/kg) mixture. Depth of anesthesia was monitored via toe pinch and supplemental doses were administered as necessary. Body temperature was maintained via a thermal probe and heating pad (Fine Science Tools). The pigeons were placed in a stereotaxic apparatus with ear bars and beak adapter such that the orientation of the head conformed to the atlas of Karten and Hodos (1967). Sufficient bone and dura was removed to allow access to the VbC. Glass micropipettes with tip diameters of 4–5 μm filled with 2 M NaCl were used for the extracellular recordings. Micropipettes were advanced through the VbC via an hydraulic microdrive (Frederick Haer). The extracellular signal was amplified, filtered, and fed to a data acquisition unit [Cambridge Electronic Designs (CED) 1401*plus*]. The data were analyzed off-line using Spike2 for Windows (CED). This included spike sorting and the construction of peristimulus time histograms (PSTHs).

Stimuli and stimulus presentation

The procedures for stimulus construction and presentation were essentially identical to those described in previous studies from this lab that examined the spatiotemporal tuning of nBOR and LM units (Crowder et al. 2003a,b, 2004; Wylie and Crowder 2000). All stimuli were generated by a VSG*Three* (Cambridge Research Systems) graphics computer and back-projected (InFocus LP750) onto a screen measuring 90 × 75° (width × height) that was positioned in the most responsive area of the receptive field. On identification and isolation of the CSA of P cells or a GL unit, the direction preference and approximate receptive field boundaries were qualitatively determined by moving a large (90 × 90°) hand-held visual stimulus, consisting of black bars, squiggles, and dots on a white background, throughout the visual field. Subsequently, spatiotemporal tuning was quantified using 36–42 combinations of sine-wave gratings of varying SF (0.03–2 cpd) and TF (0.03–24 cycles per second, Hz) moving in the preferred and anti-preferred direction for that unit. The contrast of the sine wave gratings was 0.95 [(luminance$_{MAX}$ − luminance$_{MIN}$)/(luminance$_{MAX}$ + luminance$_{MIN}$)] and the mean luminance was 65 cd/m^2. The refresh rate was 80 Hz. Each sweep for a particular SF/TF combination consisted of 4 s of motion in the preferred direction, a 3-s pause, 4 s of motion in the anti-preferred direction, followed by a 4-s pause. During the pauses, the stimulus was a uniform gray of the standard mean luminance. Firing rates were averaged over 2–12 sweeps, and mean firing rates for motion in the preferred and anti-preferred direction were computed over the entire 4-s motion segment. For CSA, the firing rate is typically very low, thus we tried to obtain as many sweeps as possible ($\leq$12) for each SF/TF combination. This was generally not a problem as the units are not difficult to hold for long periods of time. For GL units, the firing rate is higher ($\geq$10-fold), but the units were extremely difficult to isolate and hold for long durations. We required a minimum of two sweeps, assuming the unit was well isolated.

Quantification and illustration of spatiotemporal tuning

To graphically illustrate tuning in the spatiotemporal domain, for each unit, a contour plot of the mean firing rate as a function of SF and TF was made using Sigma Plot. TF and SF were plotted on the ordinate and abscissa, respectively, and firing rate (minus spontaneous rate) was plotted on the *z* axis. The location of maximal excitation was referred to as the primary peak of the contour plot. A peak of lesser magnitude was termed a secondary peak. Concluding that a contour plot contained a single peak versus two peaks was somewhat subjective (see contour plots in Figs. 1*B,* 2, and 3). To be classified as a secondary peak, it had to be clearly separable from the background activity and distinct from the primary peak by visual inspection, and a consistent response of >40% the magnitude of the primary peak was necessary. (The contour plots shown in Figs. 1*B* and 3*C* are representative in this regard).

To identify the precise location of the primary and secondary peaks, each peak was fit to a two-dimensional (2-D) Gaussian function using a slightly modified version of the method of Perrone and Thiele (2001)

$$G(u,\omega) = \{\exp[-(u')^2/\sigma_x^2]\}\, X\, \{\exp[-(\omega')^2/\sigma_y^2]\} + P$$

where

$$u' = (u - x)\cos\theta + (\omega - y)\sin\theta$$

$$\omega' = -(u - x)\sin\theta + (\omega - y)\cos\theta$$

where u is ln (SF), ω is ln (TF), θ is the angle of the Gaussian, (x, y) is the location of the peak of the Gaussian, σ_x and σ_y are the spread of the Gaussian in the u' and ω' dimensions, respectively, and P is a constant reflecting the spontaneous activity of the cell. σ_x, σ_y, x, y, θ, and P were optimized to minimize the sum of the mean error between the actual and G values using the solver function in Microsoft Excel. Not all of the data points from the contour plots were necessarily included in the Gaussian fits. In cases where there were two peaks in the contour plot, the points corresponding to each peak were fit separately (e.g., see Fig. 3, *C* and *D*). In addition, for some contour plots with single peaks spurious values distant from the peak were omitted (e.g., Fig. 2, *A* and *B,* and *C* and *D*).

To determine whether the CSA and GL primary peaks were located in the *fast* or *slow* regions of the spatiotemporal domain, we first used a hierarchical cluster analysis to divide a group of 118 cells from previous studies of LM and nBOR (Crowder and Wylie 2001; Crowder et al. 2003a,b; Wylie and Crowder 2000) into two groups based on the SF (x) and TF (y) of their primary peaks. (These are plotted in Fig. 4*C*). Post hoc inspection of the classification showed that the two largest clusters corresponded to *fast* and *slow* cells. We then determined a linear discriminant function to discriminate *fast* from *slow* cells using the cluster analysis results as a training set. The discriminant function was then used to calculate the posterior probabilities of *fast* or *slow* memberships for GL units and the CSA of P cells recorded in the present study. All analyses were conducted in *R* (Ihaka and Gentleman 1996). We used the hclust() function from the "stats" library, with the "Ward's" method, to perform the cluster analysis. The lda() function of the MASS library (Venables and Ripley 2002) was used for the linear discriminant analysis.

Quantification of velocity tuning

In addition to providing the location of the spatiotemporal peak, the Gaussian function was also used to evaluate velocity tuning (velocity = TF/SF) following the procedure used by Priebe et al. (2003) [a variant of a method devised by Levitt et al. (1994)]. Units showing velocity tuning would have a θ value approaching 45°. When plotted on a contour plot, the peak of a unit tuned to velocity is elongated and oriented such that it has a slope of ~1 on log–log axes. This contrasts with a unit that shows "spatiotemporal independence," i.e., it responds maximally to a given TF irrespective of the SF. Such a unit would have a nonoriented peak in the contour plot (i.e., θ approaching 0 or 90°). To evaluate whether a unit showed velocity tuning as opposed to spatiotemporal independence, the primary peak for each unit was fit to a 2-D Gaussian as described in the preceding text but with θ constrained to either 45 ° to provide the velocity-tuned prediction or to 0°/90° to provide the independent prediction. We then computed the partial correlation of the actual response with the velocity or independent prediction using the following equations

$$R_{\text{ind}} = (r_i - r_v * r_{iv})/\sqrt{((1 - r_v^2)(1 - r_{iv}^2))}$$

$$R_{\text{vel}} = (r_v - r_i * r_{iv})/\sqrt{((1 - r_i^2)(1 - r_{iv}^2))}$$

where R_{ind} and R_{vel} are the partial correlations of the actual response to the independent and velocity predictions, respectively; r_i is equal to the correlation of actual response with the independent prediction; r_v is the correlation of the actual data with the velocity prediction; and r_{iv} is the correlation of the two predictions.

The statistical significance of R_{vel} and R_{ind} was calculated by performing a Fisher Z-transform on the correlation coefficients {$Zf = 1/2^{\times}\ln[(1 + R)/(1 - R)]$}, and then calculating the difference between these z scores (Papoulis 1990)

$$z_{\text{diff}} = (Zf_v - Zf_i)/((1/(N_v - 3)) + 1/(N_i - 3))1/2$$

where Zf_v is the Fisher Z-transform for R_{vel}, Zf_i is the Fisher Z-transform for R_{ind}, and $N_v = N_i$ = number of SF/TF combinations used in the best-fit Gaussian. With this statistic, cells were categorized as velocity-tuned if $z_{diff} \geq 1.65$ and R_{vel} was significantly >0. Likewise cells were categorized as independent if $z_{diff} \leq -1.65$ and R_{ind} was significantly >0. Cells not meeting these criteria were termed unclassifiable ($1.65 > z_{diff} > -1.65$). The conventional criterion probability of 0.1 was used (Crow et al. 1960). This criterion has been justified by the fact that this method is not a true test for statistical significance, but a convenient way to reduce data (see Gizzi et al. 1990; Movshon et al. 1985; Scannell et al. 1996).

Histology

In some cases, dye spots were made at recording sites in the granular layer via iontophoretic injection of pontamine sky blue. At the end of these experiments, animals were given a lethal overdose of pentobarbital sodium (100 mg/kg) and immediately perfused with ice-cold saline followed by 4% paraformaldehyde in phosphate buffer (PB). The brains were extracted and postfixed (4% paraformaldehyde

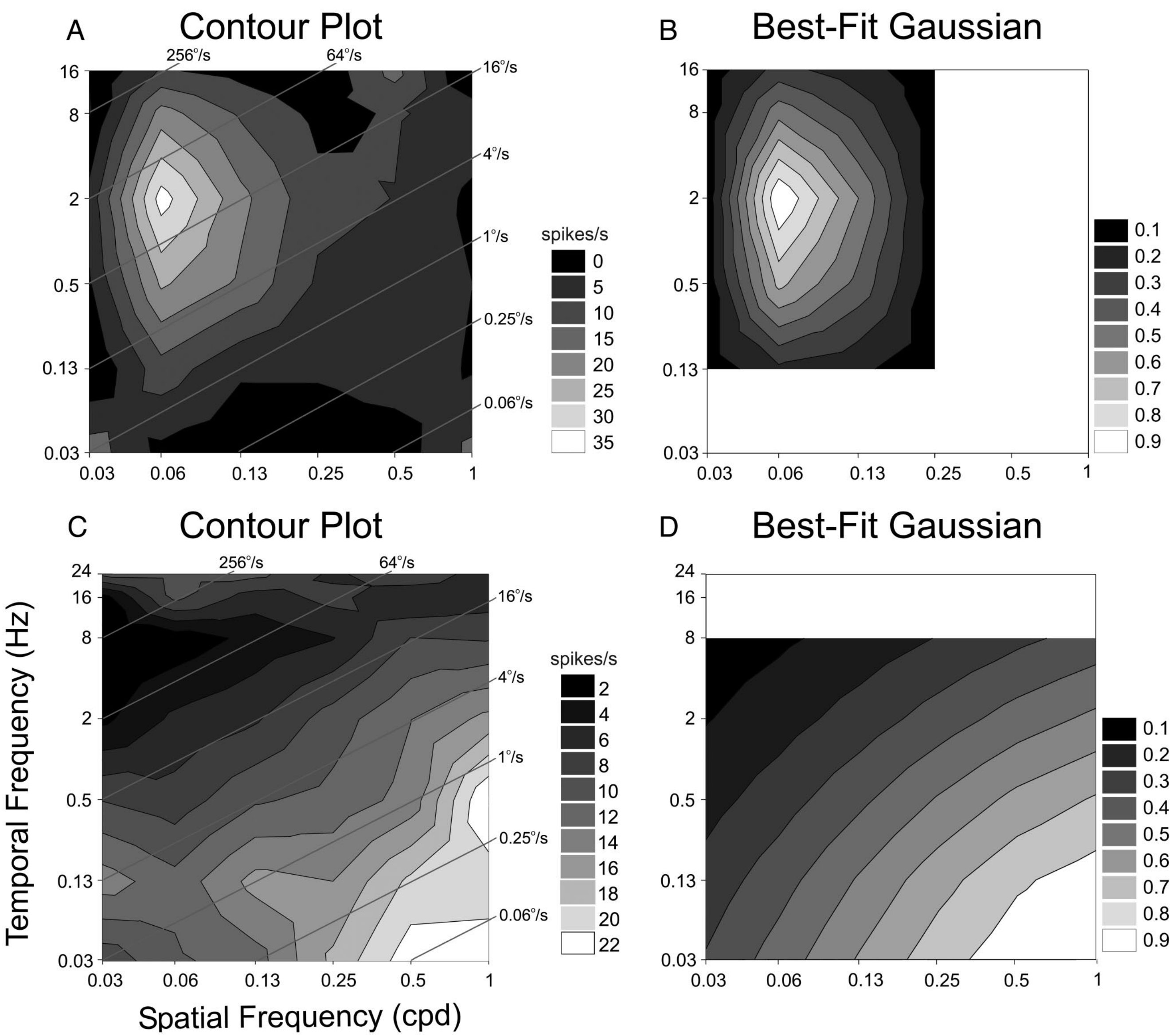

FIG. 2. Contour plots and best-fit Gaussians for representative granular layer (GL) units. *A*: the contour plot of the spatiotemporal tuning of a fast GL unit with a single peak. *B*: the plot of the normalized Gaussian for the unit in *A* as determined using the slightly modified equation of Perrone and Thiele (2001). *C* and *D*: the contour plot and best-fit Gaussian plot, respectively, of the spatiotemporal tuning of a GL unit with a single peak in the slow zone. See caption to Fig. 1 and text for additional details.

in PB with 30% sucrose) for 2–12 h and then placed in 30% sucrose solution in PB for 12–24 h. Frozen coronal sections (40 μm thick) through VbC were collected and mounted onto gelatin-coated slides. Sections were counterstained with neutral red and light microscopy was used to localize dye spots.

RESULTS

We recorded the spatiotemporal tuning of 17 GL units and the CSA of 39 P cells in VbC from 19 birds in this study. CSA was recorded in the molecular layer of folia IXcd and X, and displayed the characteristic low spontaneous activity of $\sim$1 spikes/s [0.98 $\pm$ 0.11 (SE) spikes/s]. Visually sensitive GL units were extremely difficult to isolate and hold but were easily distinguished from CSA by a much higher spontaneous rate (26.10 $\pm$ 3.68 spikes/s). The dye spots made at GL recording sites were all located in the granular layer of folia IXc,d. As expected, in response to the battery of drifting sine wave gratings, CSA and visual GL units showed clear spatiotemporal tuning.

Spatiotemporal tuning of GL units

Consistent with previous studies, only a fraction ($<$10%) of the GL units were modulated by optic flow stimuli (Fan et al. 1993; Waespe et al. 1981). Moreover, consistent with Wylie et al. (1993), we found that the visual GL units had monocular receptive fields in either the ipsilateral (n = 11) or contralateral (n = 6) visual field and showed directional tuning to large-field stimuli. Different direction preferences (similar to those in LM and nBOR) were observed, but GL units with dissimilar direction selectivity did not have any apparent differences with respect to spatiotemporal tuning.

Figure 1*B* shows a contour plot illustrating the spatiotemporal tuning of a GL unit. This unit had a primary peak in the fast zone, and a slightly smaller secondary peak in the slow zone. Based on the best-fit Gaussian, the primary peak was localized to SF = 0.10 cpd, TF = 13.47 Hz and the secondary peak was located at SF = 1.0 cpd, TF = 0.28 Hz. PSTHs on the right show the unit's modulation during stimulation in the preferred and antipreferred direction for gratings of three different SF–TF combinations during a single sweep. The first 4 s show response to movement in the preferred direction, followed by a 3-s pause, 4 s of motion in the anti-preferred direction, and another 3-s pause. Clear excitation and inhibition to motion in the preferred and anti-preferred direction, respectively, are seen for PSTHs in the primary peak (SF = 0.125 cpd, TF = 16 Hz) and secondary peak (SF = 1 cpd, TF = 0.5 Hz), although this modulation is clearly greater for the primary peak. Considerably less modulation is seen outside these peaks (i.e., SF = 0.25 cpd, TF = 2 Hz). Evident in the PSTHs, the responses included both transient and steady-state components. (This was the also the case for CSA). Transients and other temporal factors have been extensively analyzed in previous studies of spatiotemporal tuning in the AOS and pretectum (Ibbotson et al. 1994; Price and Ibbotson 2002; Wolf-Oberhollenzer and Kirschfeld 1994) and will not be analyzed further in this paper.

Figure 2 shows the contour plots of the spatiotemporal tuning of two additional GL units. The unit in Fig. 2*A* showed a single peak in the *fast* region. Figure 2*B* shows the plot of the normalized best-fit Gaussian for this unit. The peak was located at SF = 0.06 cpd, TF = 2.03 Hz. Figure 2, *C* and *D,* shows the contour plot and normalized best-fit Gaussian, respectively, for a GL unit with a single peak in the *slow* zone (SF = 1.0 cpd, TF = 0.03 Hz). Eight (47.1%) GL units had a single peak in the contour plot (as in Fig. 2), whereas nine of the GL units (52.9%) had secondary peaks in their contour plots (as in Fig. 1*B*). Secondary peaks were always located in the opposite spatiotemporal domain and had a magnitude, on average, 73.4% the size of the primary peak (range, 43.4–98.5%).

Figure 4*A* plots the locations of the primary peaks of all 17 GL units as determined from the best-fit Gaussians. As described in METHODS, the locations of the peaks were assigned to either the fast or slow regions based on previous data of spatiotemporal tuning of LM and nBOR neurons (Crowder and Wylie 2001; Crowder et al. 2003a,b; Wylie and Crowder 2000). In Fig. 4*C* the primary peaks of nBOR and LM neurons is plotted along with data from the current study. Eight (47.1%) GL units were classified as *fast* cells (low SFs/high TFs; mean = 0.13 cpd/8.24 Hz), whereas nine (52.9%) GL units were *slow* cells (high SFs/low TFs; mean = 0.68 cpd/0.30 Hz; see also Table 1). The clustering into fast (white diamonds) and slow (gray diamonds) groups can be clearly seen in Fig. 4*A* (see also Fig. 4*C*).

Figure 5, *A* and *B,* shows the normalized average contour plots of spatiotemporal tuning for *slow* and *fast* GL units, respectively. These were calculated by normalizing the contour plot of each unit, then averaging across all nine slow units and eight fast units. While the *slow* units clearly respond maximally to the gratings in the *slow* region, and the *fast* units clearly respond more to *fast* gratings, note the influence of the subset of units (9 GL units) that had secondary peaks in the region opposite the primary peak. Five *fast* units had secondary peaks in the *slow* zone and four *slow* units had secondary peaks in the *fast* regions.

Spatiotemporal tuning of the CSA of Purkinje cells

Previous studies in pigeons have shown that VbC Purkinje cells have binocular, virtually panoramic receptive fields, and the CSA responds best to optic flow patterns resulting from self-translation or self-rotation along/about a particular axis in three-dimensional space (Wylie and Frost 1993, 1999; Wylie et al. 1998). Based on the orientation of the preferred axis of rotation/translation, there are two classes of rotation neurons and four classes of translation neurons. Rotation-sensitive neurons in VbC respond best to optic flow rotating about either the vertical axis (VA) or an axis orientated 45^o contralateral to the midline in the horizontal plane (45^o c azimuth). Translation-sensitive neurons respond best to translational optic flow moving upward or downward along the VA, forward along an axis at 45^o c azimuth or backward along an axis orientated at 45^o ipsilateral azimuth. In the present study, all six classes were represented in the sample of 39 units (24 rotation neurons, and 15 translation neurons). The different groups did not differ with respect to spatiotemporal tuning, thus they have all been grouped together.

Figure 3 shows representative contour plots and best-fit Gaussians for the CSA of two Purkinje cells. In Fig. 3, *A* and *B*, a cell with a single peak in the slow domain of the contour plot is illustrated. From the best-fit Gaussian, the peak was located at SF = 0.66 cpd, TF = 0.18 Hz. In Fig. 3, *C* and *D,* a cell with a primary peak in the *slow* zone and a secondary peak in the *fast* zone is shown. From the best-fit Gaussian the primary peak was located at 0.77 cpd/0.10 Hz and the secondary peak was located at 0.11 cpd/18.0 Hz. Of the 39 CSA

TABLE 1. *Preferred spatial frequencies (SFs), temporal frequencies (TFs), and velocities of fast and slow neurons*

	Fast Cells				*Slow* Cells			
	n (% total)	SF, cpd	TF, Hz	Velocity, °/s	*n* (% total)	SF, cpd	TF, Hz	Velocity, °/s
Pigeon nBOR	13 (25)	0.078	2.84	36.2* [70.8†]	40 (75)	0.53	0.30	0.57* [0.75†]
Pigeon LM	23 (66)	0.10	2.49	25.8* [52.3†]	12 (34)	0.67	0.55	0.82* [1.08†]
Pigeon GL unit	8 (47)	0.13	8.24	63.4* [69.8†]	9 (53)	0.68	0.30	0.4* [0.5†]
Pigeon CSA	1 (3)	0.10	0.55	5.5* [5.5†]	38 (97)	0.67	0.35	0.5* [0.5†]

Average SFs, TFs, and velocities of the primary peaks are shown for the *fast* and *slow* neurons in the pigeon nucleus of the basal optic root (nBOR) (Crowder et al. 2003a) and lentiformis mesencephali (LM) (Wylie and Crowder 2000) and granular layer (GL) units and the complex spike activity (CSA) of Purkinje cells in the vestibulocerebellum (present study). Percentages are in parentheses. *, arithmetic mean; †, mean TF/mean SF.

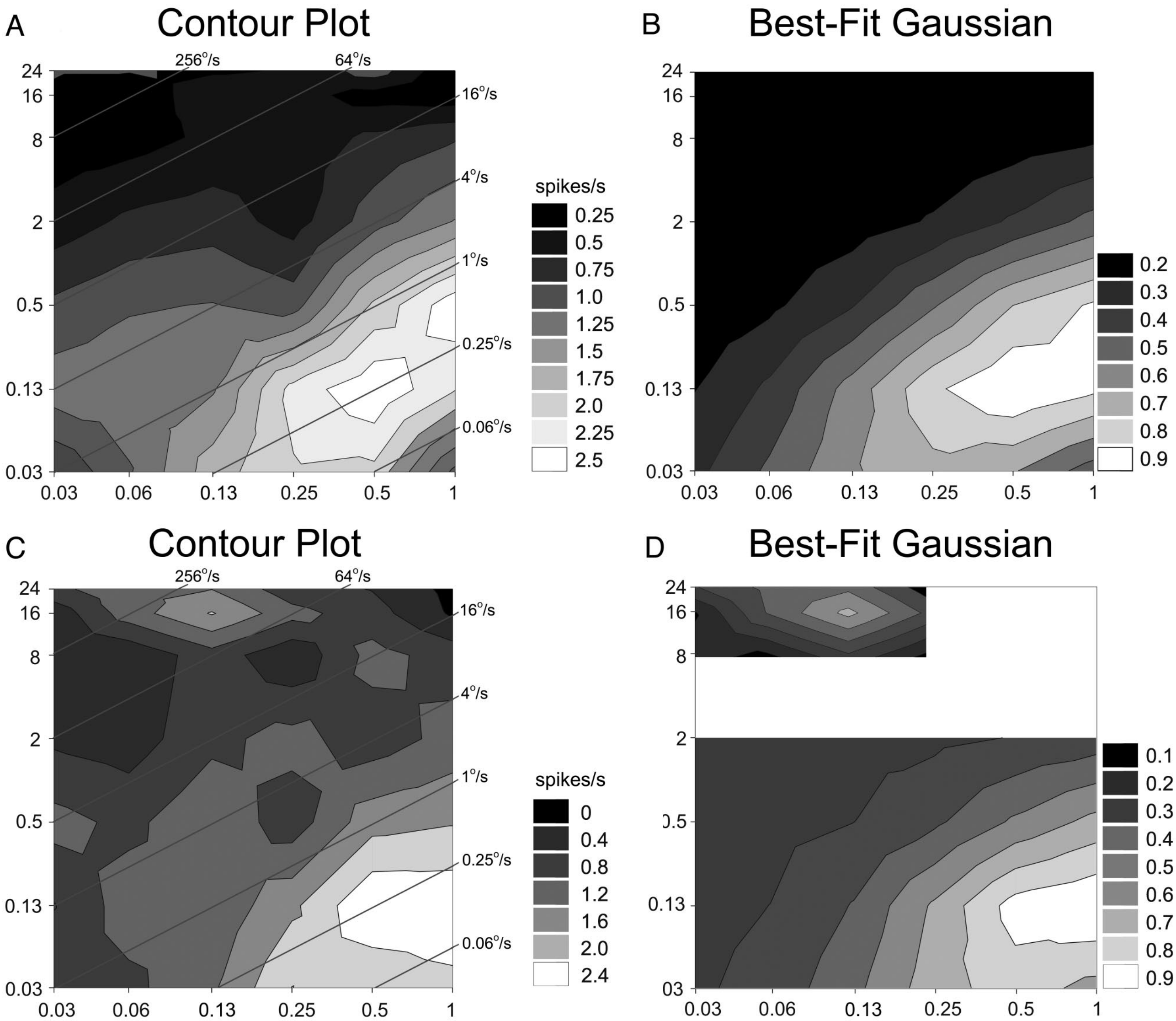

FIG. 3. Contour plots and Gaussian plots for the complex spike activity of representative Purkinje cells (CSA of P cells). *A*: the contour plot of the spatiotemporal tuning of a P cell with a single peak in the slow zone. *B*: the plot of the normalized 2-dimensional (2-D) Gaussian for the unit in *A*. In *C*, a P cell with a primary peak in the slow zone and a secondary peak in the fast zone is shown. The normalized 2-D Gaussian for this unit is plotted in *D*. See captions to Figs. 1 and 2 and the text for additional details.

recordings, 11 (28.2%) of the contour plots showed a single peak, whereas 28 (71.8%) showed a secondary peak as well. On average, the secondary peak was 69.8% (range, 51.2–97.9%) the size of the primary peak. For two of these units, the magnitude of the secondary peak was >90% of the primary peak, making the assignment of primary and secondary peak more problematic.

Figure 4*B* plots the locations of the primary peaks of the CSA of 39 P cells in this study. These are also plotted in Fig. 4*C* along with the GL units and the nBOR and LM data from previous studies (Crowder and Wylie 2001; Crowder et al. 2003a,b; Wylie and Crowder 2000). Using the linear discriminate function described previously, 38 (97.4%) of the CSA units were classified as *slow* units (mean = 0.67 cpd/0.35 Hz; Fig. 4*A*, ●), whereas one unit was classified as a *fast* unit (Fig. 4*C*, ○, primary peak at 0.10 cpd/0.55 Hz). This *fast* unit had a secondary peak of approximately equal magnitude (96.5%) located in the *slow* zone (0.42 cpd/0.43 Hz). Twenty seven of the 38 *slow* units had secondary peaks, and 25 of these were in the *fast* region.

Figure 5*C* shows the normalized average contour plots of spatiotemporal tuning for the CSA of all 39 P cells. The average plots clearly illustrate the dominance of *slow* spatiotemporal tuning in CSA, though the influence of secondary peaks in a subset of CSA (71.8%) is apparent with the smaller peak in the *fast* region. Note the similarity of the contour plots for the *slow* GL units and the CSA. Note also that the peaks for the *slow* GL units and CSA are sharper than that of the *fast* units, reflecting the fact that for the *fast* units the primary peaks are not as tightly clustered (Fig. 4*A*).

Velocity-like tuning

In Fig. 3*A*, note that peak for this unit is elongated and oriented such that it has a slope of ~1 on a log–log axis. This suggests that the cell shows velocity tuning (velocity = TF/SF) to ~0.25 °/s (see diagonal scale on the contour plot). As the response is not independent of SF, this has been more appropriately termed velocity-like tuning (Crowder et al. 2003a; Zanker et al. 1999). In the present study, many of the peaks that were in the slow zone were oriented such that they approached velocity-like tuning (e.g., Figs. 1*B,* 2*C,* and 3*A*). As described in METHODS, following Priebe et al. (2003), neurons were classified as velocity tuned, independent, or unclassified based on the partial correlations of the actual data for each unit to velocity and independent predictions. Using the criteria described in the methods, the CSA of 10 (26.3%) slow P cells showed velocity-like tuning, 5 (13.2%) showed independence, and 23 (60.5%) fell into the unclassified group. The single fast CSA was also unclassified. For the eight fast GL units, 4 (50%) showed SF/TF-independence, 1(12.5%) was velocity-tuned and three (37.5%) were in the unclassified group. For the nine slow GL units, all fell into the unclassified group.

Figure 6 shows a scatter plot of R_{vel} versus R_{ind} for all units. For convenience, — has been added to provide an approximation of the divisions between velocity-tuned, unclassified, and independent regions. This line represents the statistical criteria separating these groups based on 24 points in the best-fit Gaussian. [The actual number of points in the best-fit Gaussians ranged from 12 to 42 (mean = 24), hence this line is an approximation between the divisions]. Note the CSA that showed velocity tuning in the top left (●) and the *fast* GL units that showed SF/TF-independence in the bottom right (◇).

DISCUSSION

In this study, we examined the spatiotemporal tuning of the CSA of VbC Purkinje cells and GL units in folium IXcd of the VbC in response to largefield sine-wave gratings of varying SF and TF drifting in the preferred direction. We found that these units were tuned in the spatiotemporal domain. GL units could be classified into two groups: *fast* units showed a maximal response to low SF/high TF gratings, whereas *slow* units showed a maximal response to high SF/low TF. In contrast, all but one of the CSA recordings was classified as a *slow* unit.

Comparison with spatiotemporal tuning in the pretectum and AOS

Spatiotemporal tuning in the optokinetic system was originally demonstrated by Ibbotson et al. (1994), who recorded from the pretectum in wallabies. Subsequently, Wylie and Crowder (2000) showed strikingly similar results in the pretectal nucleus LM and the nBOR of the AOS in pigeons (Crowder and Wylie 2001; Crowder et al. 2003a,b; Wolf-Oberhollenzer and Kirschfeld 1994). The results from these previous studies closely parallel those in this study. Like CSA and GL units, LM and nBOR neurons had a primary peak located in either the *fast* or *slow* zone. In LM, *fast* units were

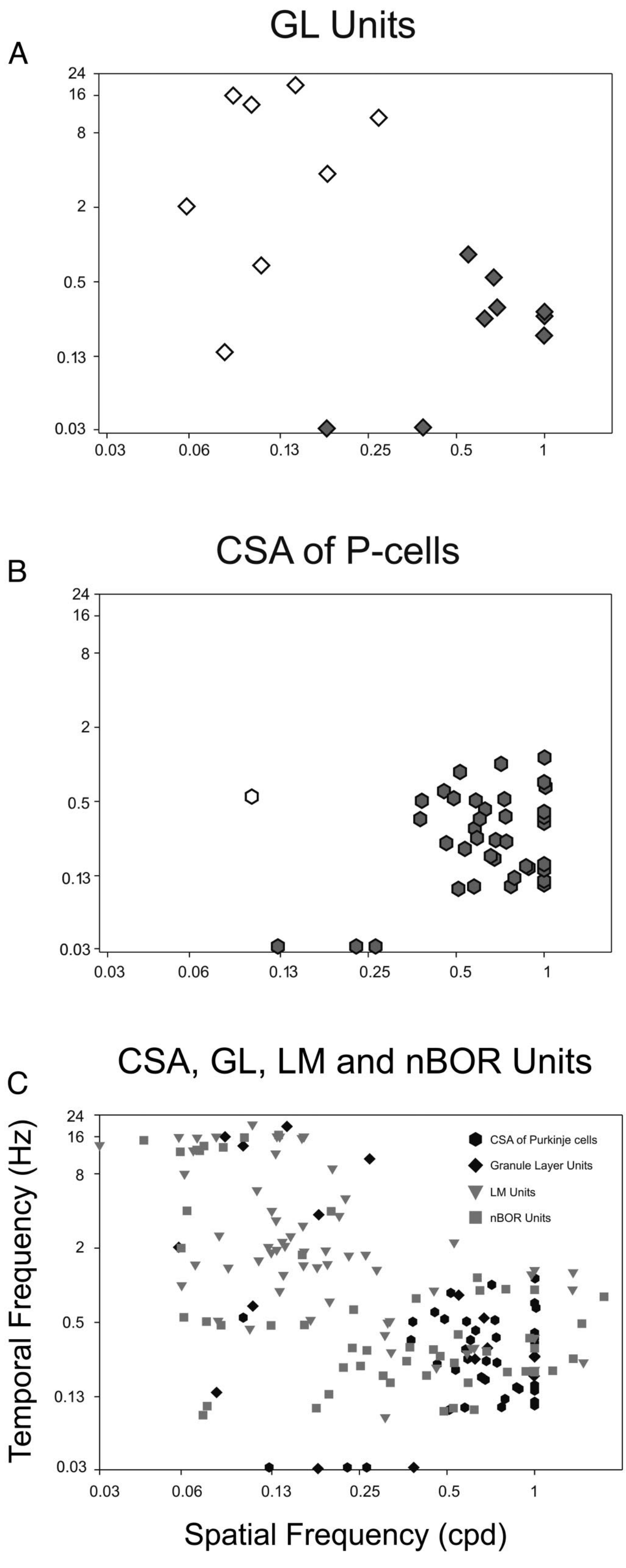

FIG. 4. Spatiotemporal tuning of GL units and the CSA of P cells. In these plots, the primary peak locations in the spatiotemporal domain for all GL units (*A*) and the CSA of all P cells (*B*) are indicated. In *A,* 8 of the units had a primary peak in the fast spatiotemporal domain (◇), whereas 9 had a primary peak in the slow zone (◆). In *B,* 38 of the 39 peaks fall within the slow zone (●). The remaining P cell had a primary peak at 0.10 cpd/0.55 Hz (○). In *C,* data from the current study of the VbC and previous studies of spatiotemporal tuning in lentiformis mesencephali (LM) and nucleus of the basal optic root (nBOR) is collapsed onto a single plot: ● the primary peak locations of the CSA of 39 P cells in VbC (present study); ◆, primary peak locations for 17 GL units in VbC (present study); ▼, the primary peaks of 64 LM units (Wylie and Crowder 2000); ▨ and the primary peaks of 55 units from nBOR (Crowder and Wylie 2001; Crowder et al. 2003a). See text for details.

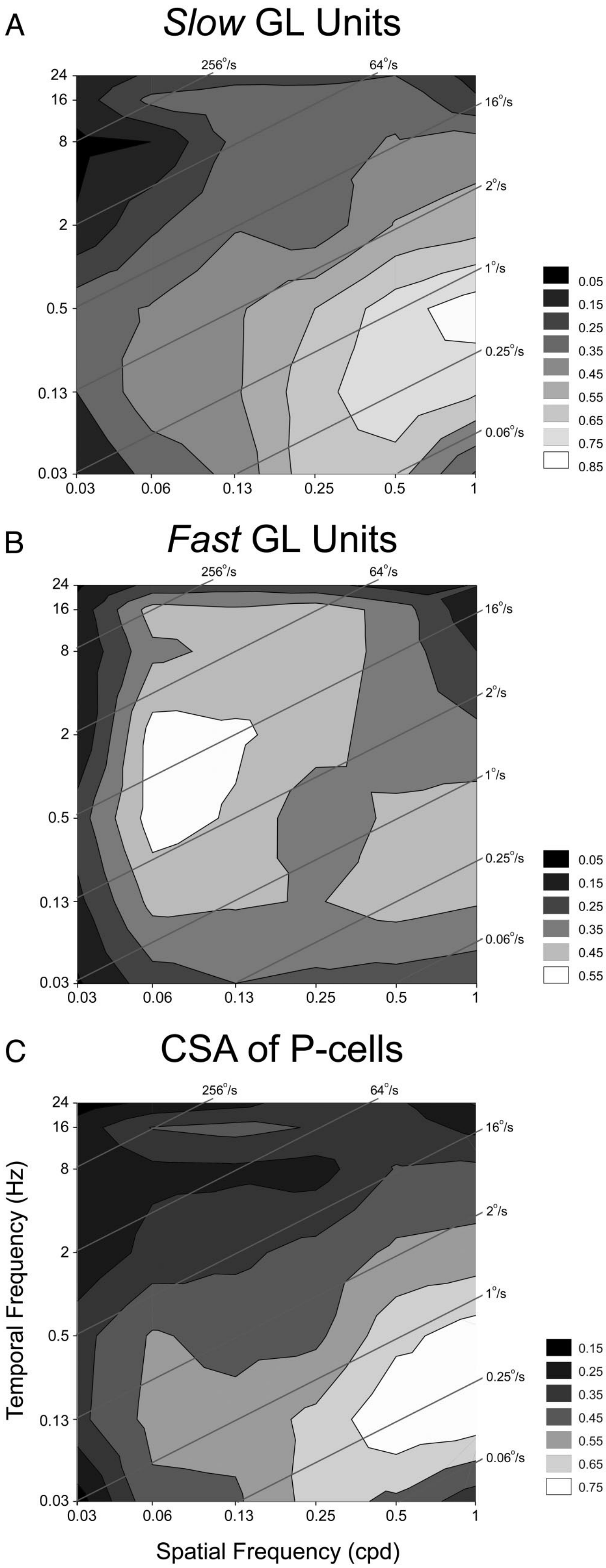

FIG. 5. Normalized average contour plots of spatiotemporal tuning. *A–C*: the normalized average plots, respectively, for the 9 slow GL units, 8 fast GL units, and CSA of 39 P cells recorded in this study. See captions for Figs. 1–4 and text for additional details.

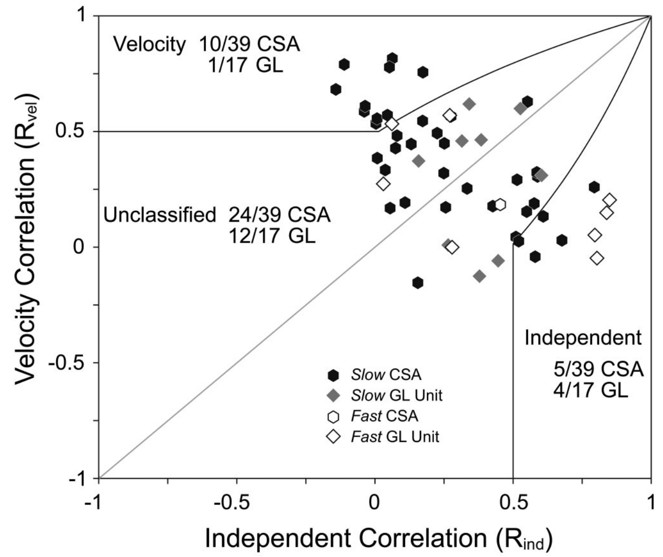

FIG. 6. Scatter plots of partial correlations for velocity (R_{vel}) and spatiotemporally independent (R_{ind}) tuning. Each data point indicates the degree to which a particular GL unit or the CSA of a P cell are correlated with velocity and SF/TF-independent predictions. The data space is divided into three regions based on statistical criteria approximated by the solid black lines. Velocity tuned, unclassifiable, or spatiotemporally independent cells fall in the top left, middle, or bottom right areas of the scatter plot, respectively. ●, slow CSA; ◆, slow GL units; ○, fast CSA; and ◇, fast GL. Slow CSA was velocity tuned in 10 instances, while a single fast GL unit showed velocity tuning. See text for additional details.

more common than *slow* units (66 vs. 34%), but in nBOR, *slow* units were more common than *fast* units (75 vs. 25%). In the present study, we found that GL units included *fast* and *slow* units, whereas CSA was clearly tuned to *slow* gratings. Table 1 summarizes the mean preferred SF/TF combinations from studies of LM, nBOR, and the VbC of pigeons (Crowder and Wylie 2001; Crowder et al. 2003a; Wylie and Crowder 2000; present study). The average preferred SF/TF combinations for the *slow* units in LM and nBOR were 0.67 cpd/0.55 Hz and 0.53 cpd/0.30 Hz, respectively (Crowder and Wylie 2001; Crowder et al. 2003a; Wylie and Crowder 2000), which is quite close to the values for the *slow* GL units (0.68 cpd/0.30 Hz) and CSA (0.67 cpd/0.35 Hz) in the present study. Likewise, the average preferred SF/TF combinations for the *fast* units in LM and nBOR were 0.10 cpd/2.49 Hz and 0.08 cpd/2.84 Hz, respectively (Crowder et al. 2003a; Wylie and Crowder 2000), which is close to the values for the *fast* GL units (0.13 cpd/8.24 Hz) from the present study. In Fig. 4*C,* data from the current study of the VbC and previous studies of spatiotemporal tuning in LM and nBOR are collapsed onto a single plot: ● show the primary peak locations in the spatiotemporal domain of recordings of the CSA of P cells in VbC ($n = 39$; present study); ◆ show primary peak locations for GL units in VbC ($n = 17$; present study); ▼ show the primary peaks of LM units ($n = 64$) (Wylie and Crowder 2000); and the primary peaks of units from nBOR ($n = 55$) are represented by ▨ (Crowder and Wylie 2001; Crowder et al. 2003a). The *fast* and *slow* populations form distinct clusters. The distribution of primary peaks within the *fast* and *slow* regions is similar for LM, nBOR, and VbC units.

In the present study, we also found that the many of the contour plots of GL unit responses and CSA often included secondary peaks, almost always in the opposite region. This was also the case for many nBOR and LM neurons (Crowder and Wylie 2001; Crowder et al. 2003a; Wylie and Crowder 2000) and some NOT neurons in wallabies (Ibbotson et al. 1994).

Projections of fast and slow neurons in the AOS and pretectum to the VbC

Figure 7 shows a cartoon of the projections of the nBOR and LM to the VbC. There is an indirect CF pathway through the medial column of the inferior olive (mcIO) (Arends and Voogd 1989; Brecha et al. 1980; Clarke 1977; Crowder et al. 2000; Gamlin and Cohen 1988; Lau et al. 1998; Winship and Wylie 2001, 2003; Wylie 2001; Wylie et al. 1999) and a direct MF pathway that is restricted to folium IXcd (Brauth and Karten 1977; Brecha and Karten 1979; Brecha et al. 1980; Clarke 1977; Gamlin and Cohen 1988; Wylie and Linkenhoker 1996; Wylie et al. 1997). Our results suggest that the *slow* neurons in LM and nBOR make up the primary input to the CF pathway, whereas the MF pathway receives major inputs from *fast* and *slow* neurons in LM and nBOR. This is not to say that the CSA does not respond to *fast* gratings. Clearly many of the units have a secondary peaks in the *fast* region of the contour plot (Fig. 3*C;* see also Fig. 5*C*) as do many *slow* neurons in LM and nBOR (Crowder and Wylie 2001; Crowder et al. 2003a; Wylie and Crowder 2000), thus there is clearly an integration of *fast* and *slow* information in the CF pathway. Nonetheless we contend that the CF pathway receives input almost exclusively from cells in nBOR and LM that are maximally sensitive to *slow* gratings.

Although the CF pathway from the AOS and pretectum to the VbC exists in all mammals (for reviews, see Simpson 1984; Simpson et al. 1988), a direct MF projection from the AOS and pretectum to the VbC has not been identified in mammals with the possible exception of a controversial MTN–VbC projection in the chinchilla (Winfield et al. 1978). However, there may be several indirect MF pathways from the pretectum and AOS to the VbC. Most of the MF input to the VbC arises in the vestibular nuclei and the prepositus hypoglossi (Ruigrok 2003; Voogd et al. 1996), but there are also projections originating in the reticular formation, the raphe nuclei, and neurons located within and around the medial longitudinal fasciculus (Blanks et al. 1983; Gerrits et al. 1984; Langer et al. 1985; Ruigrok 2003; Sato et al. 1983; for review, see Voogd et al. 1996). The NOT and the AOS project to many of these structures, including the vestibular nuclei, the medial and dorsolateral nuclei of the basilar pontine complex, the mesencephalic reticular formation, the prepositus hypoglossi, and the nucleus reticularis tegmenti pontis (Cazin et al. 1982; Giolli et al. 1984, 1985, 1988; Holstege and Collewijn 1982; Itoh 1977; Terasawa et al. 1979; Torigoe et al. 1986a,b; for review, see Simpson et al. 1988). Thus it is possible that optic-flow information reaches the VbC from the AOS and pretectum via an indirect MF pathway in mammalian species. It would be interesting to see if this information arises from *fast* and/or *slow* neurons.

Function of fast and slow neurons

Ibbotson et al. (1994) described the potential role of the *slow* and *fast* NOT neurons in the generation and maintenance of OKN. The *fast* units would respond maximally when retinal slip velocity (RSV) is high, whereas the *slow* neurons would be involved when the RSV is low, such as providing the error signal when the OKN gain is high (see Ibbotson et al. 1994 and Wylie and Crowder 2000 for detailed discussions). From the findings of the present study, it follows that the MF inputs are involved when RSV is high and low, but the CF inputs are primarily involved when RSV is low. However, again we caution against such a stark simplification: the contour plots of many of the CSA recordings showed a secondary peak in the *fast* zone. Thus the CSA of these Purkinje cells would not be silent to *fast* optic flow stimuli.

Velocity-like tuning versus spatiotemporal independence

In the present study, we found that many of the peaks in the *slow* zone were oriented such that they had a slope approximating one on log–log axes. That is, these units showed a peak response to a particular stimulus velocity (TF/SF), irrespective of the SF used. As the response maxima were dependent on SF, we (Crowder et al. 2003a) have previously called this velocity-like tuning (true velocity tuning would appear as a flattened ridge in the contour plot). Crowder et al. (2003a) concluded that the majority of the *slow* units in LM and nBOR showed velocity-like tuning, whereas the *fast* units were TF tuned (i.e., SF/TF-independent). However, Crowder et al. (2003a) did not provide a quantitative test in this regard, and one can infer from Priebe et al. (2003) that there is a danger in overstating the degree of velocity-like tuning. Thus we adopted the partial correlation outlined by Priebe et al. (2003) to compare velocity-tuned and SF/TF-independent predictions. The tendency of slow CSA to show velocity tuning is apparent in Fig. 6, but only 26% showed significant velocity tuning compared with the independence prediction; 13.1% showed significant SF/TF-independence, but most (60.5%) fell into the unclassified group, i.e., somewhere between velocity tuning and SF-TF-independence. Consistent with Crowder et al. (2003a), SF/TF-independence was more common with the fast GL units (50%). Following Zanker et al. (1999), Crowder et al. (2003a) argued that velocity-like tuning reflects the properties of an "unbal-

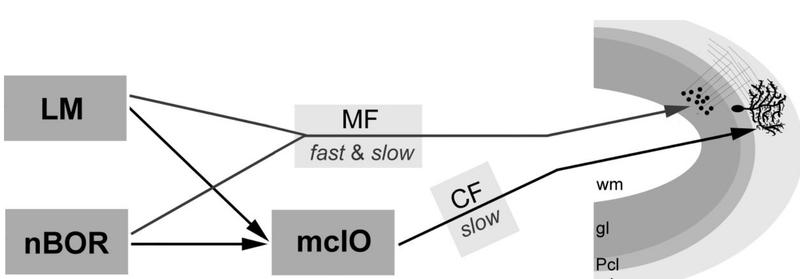

FIG. 7. Optic flow input from the accessory optic system (AOS) and pretectum to the VbC in pigeons. This schematic illustrates the mossy fiber (MF) and climbing fiber (CF) inputs arriving at the VbC from the retinal recipient nuclei of the AOS (nBOR) and pretectum (lentiformis mesencephali, LM) and the medial column of the inferior olive (mcIO), respectively. The results of this study indicate that the CF input to Purkinje cells in the VbC is primarily from slow cells in LM and nBOR, whereas MF input to the granular layer arises in both fast and slow cells in LM and nBOR. ml, molecular layer; Pcl, Purkinje cell layer; wm, cerebellar white matter.

anced" Reichardt detector. Generally speaking, the more unbalanced the detector, the more the response approaches velocity tuning. Thus with respect to velocity tuning versus SF/TF-independence, the responses we observed suggest that the input units might vary with respect to the degree to which the detector is balanced.

GL units: granule cells or MF rosettes?

There is precious little data regarding the physiological properties of MF inputs to the granule cell layer, presumably because these cells are small and difficult to isolate and hold. In fact, it is unclear whether the GL units recorded in the present study represent MF rosettes or granule cells. This is not necessarily a critical issue for the present study, as recordings from either would allow us to determine if *fast* or *slow* units in the pretectum and AOS feed the MF pathway to the VbC. Fan et al. (1993) and Ariel and Fan (1993) recorded the visual responses of units in the GL in the turtle cerebellum using an in vitro preparation with eyes attached. Similar to pigeons (Wylie et al. 1993; present study), these units exhibited direction selectivity to large-field patterns but only respond to stimulation of the contralateral eye. Based on the following responses to stimulation of the nBOR, Ariel and Fan (1993) concluded that at least some (6/15) of the units they recorded were MF rosettes as opposed to granule cells. A recent study in rats using whole cell patch-clamp recordings showed that granule cells exhibited a low firing rate in vivo with the mean spontaneous firing rate in the absence of holding current being 0.5 ± 0.2 Hz (Chadderton et al. 2004). Based on this, it is likely that the GL units in the present study, which had high spontaneous rates (average $= 26.10 \pm 3.68$ spikes/s), represent recordings from the MF rosettes in the granular layer.

GRANTS

This research was supported by funding from the Natural Sciences and Engineering Research Council of Canada (NSERC) to D.R.W. Wylie and P. L. Hurd. D.R.W. Wylie was supported by the Canada Research Chairs Program. I. R. Winship was supported by graduate fellowships from NSERC and the Alberta Heritage Foundation for Medical Research.

REFERENCES

Arends JJA and Voogd J. Topographic aspects of the olivocerebellar system in the pigeon. *Exp Brain Res Suppl* 17: 52–57, 1989.

Ariel M and Fan TX. Electrophysiological evidence for a bisynaptic retinocerebellar pathway. *J Neurophysiol* 69: 1323–30, 1993.

Ariel M and Kogo N. Direction tuning of inhibitory inputs to the turtle accessory optic system. *J Neurophysiol* 86: 2919–2930, 2001.

Blanks RH, Precht W, and Torigoe Y. Afferent projections to the cerebellar flocculus in the pigmented rat demonstrated by retrograde transport of horseradish peroxidase. *Exp Brain Res* 52: 293–306, 1983.

Brauth SE and Karten HJ. Direct accessory optic projections to the vestibulocerebellum: a possible channel for oculomotor control systems. *Exp Brain Res* 28: 73–84, 1977.

Brecha N and Karten HJ. Accessory optic projections upon oculomotor nuclei and vestibulocerebellum. *Science* 203: 913–916, 1979.

Brecha N, Karten HJ, and Hunt SP. Projections of the nucleus of basal optic root in the pigeon: An autoradiographic and horseradish peroxidase study. *J Comp Neurol* 189: 615–670, 1980.

Burns S and Wallman J. Relation of single unit properties to the occulomotor function of the nucleus of the basal optic root (AOS) in chickens. *Exp Brain Res* 42: 171–180, 1981.

Carpenter RHS. *Movements of the Eye* (2nd ed.). London: Pion, 1988.

Cazin L, Magnin M, and Lannou J. Non-cerebellar visual afferents to the vestibular nuclei involving the prepositus hypoglossal complex: an autoradiographic study in the rat. *Exp Brain Res* 48: 309–313, 1982.

Chadderton P, Margrie TW, and Hausser M. Integration of quanta in cerebellar granule cells during sensory processing. *Nature* 428: 856–860, 2004.

Clarke PGH. Some visual and other connections to the cerebellum of the pigeon. *J Physiol* 243: 267–285, 1977.

Collewijn H. Direction-selective units in the rabbit's nucleus of the optic tract. *Brain Res* 100: 489–508, 1975a.

Collewijn H. Oculomotor areas in the rabbit's midbrain and pretectum. *J Neurobiol* 6: 3–22, 1975b.

Crow EL, Davis FA, and Maxfield MW. *Statistics Manual, With Examples Taken from Ordinance Development.* New York: Dover, 1960.

Crowder NA, Dawson MR, and Wylie DR. Temporal frequency and velocity-like tuning in the pigeon accessory optic system. *J Neurophysiol* 90: 1829–41, 2003a.

Crowder NA, Dickson CT, and Wylie DR. Telencephalic input to the pretectum of pigeons: an electrophysiological and pharmacological inactivation study. *J Neurophysiol* 91: 274–85, 2004.

Crowder NA, Lehmann H, Parent MB, and Wylie DR. The accessory optic system contributes to the spatio-temporal tuning of motion-sensitive pretectal neurons. *J Neurophysiol* 90: 1140–51, 2003b.

Crowder NA, Winship IR, and Wylie DR. Topographic organization of inferior olive cells projecting to translational zones in the vestibulocerebellum of pigeons. *J Comp Neurol* 419: 87–95, 2000.

Crowder NA and Wylie DRW. Fast and slow neurons in the nucleus of the basal optic root in pigeons. *Neurosci Let* 304: 133–136, 2001.

Distler C and Hoffmann KP. Visual receptive field properties in kitten pretectal nucleus of the optic tract and dorsal terminal nucleus of the accessory optic tract. *J Neurophysiol* 70: 814–827, 1993.

Fan TX, Rosenberg AF, and Ariel M. Visual-response properties of units in the turtle cerebellar granular layer in vitro. *J Neurophysiol* 69: 1314–22, 1993.

Fan TX, Weber AE, Pickard GE, Faber KM, and Ariel M. Visual responses and connectivity in the turtle pretectum. *J Neurophysiol* 73: 2507–2521, 1995.

Finger TE and Karten HJ. The accessory optic system in teleosts. *Brain Res* 153: 144–9, 1978.

Fite KV. Pretectal and accessory-optic visual nuclei of fish, amphibia and reptiles: themes and variations. *Brain Behav Evol* 26: 71–90, 1985.

Fite KV, Kwei-Levy C, and Bengston L. Neurophysiological investigation of the pretectal nucleus lentiformis mesencephali in *Rana pipiens. Brain Behav Evol* 34: 164–170, 1989.

Gamlin PDR and Cohen DH. Projections of the retinorecipient pretectal nuclei in the pigeon (*Columba livia*). *J Comp Neurol* 269: 18–46, 1988.

Gerrits NM, Epema AH, and Voogd J. The mossy fiber projection of the nucleus reticularis tegmenti pontis to the flocculus and adjacent ventral paraflocculus in the cat. *Neuroscience* 11: 627–644, 1984.

Gibson JJ. The visual perception of object motion and subjective movement. *Psychol Rev* 61: 304–314, 1954.

Gioanni H. Stabilizing gaze reflexes in the pigeon (*Columba livia*). I. Horizontal and vertical optokinetic eye (OKN) and head (OCR) reflexes. *Exp Brain Res* 69: 567–582, 1988.

Gioanni H, Rey J, Villalobos J, Bouyer JJ, and Gioanni Y. Optokinetic nystagmus in the pigeon (*Columba livia*). I. Study in monocular and binocular vision. *Exp Brain Res* 44: 362–370, 1981.

Gioanni H, Rey J, Villalobos J, and Dalbera A. Single unit activity in the nucleus of the basal optic root (nBOR) during optokinetic, vestibular and visuo-vestibular stimulations in the alert pigeon (*Columba livia*). *Exp Brain Res* 57: 49–60, 1984.

Gioanni H, Rey J, Villalobos J, Richard D, and Dalbera A. Optokinetic nystagmus in the pigeon (*Columba livia*). II. Role of the pretectal nucleus of the accessory optic system. *Exp Brain Res* 50: 237–247, 1983a.

Gioanni H, Villalobos J, Rey J, and Dalbera A. Optokinetic nystagmus in the pigeon (*Columba livia*). III. Role of the nucleus ectomammilaris (nEM): interactions in the accessory optic system. *Exp Brain Res* 50: 248–258, 1983b.

Giolli RA, Blanks RH, and Torigoe Y. Pretectal and brain stem projections of the medial terminal nucleus of the accessory optic system of the rabbit and rat as studied by anterograde and retrograde neuronal tracing methods. *J Comp Neurol* 227: 228–251, 1984.

Giolli RA, Blanks RH, Torigoe Y, and Williams DD. Projections of medial terminal accessory optic nucleus, ventral tegmental nuclei, and substantia nigra of rabbit and rat as studied by retrograde axonal transport of horseradish peroxidase. *J Comp Neurol* 232: 99–116, 1985.

Giolli RA, Torigoe Y, Blanks RH, and McDonald HM. Projections of the dorsal and lateral terminal accessory optic nuclei and of the interstitial nucleus of the superior fasciculus (posterior fibers) in the rabbit and rat. *J Comp Neurol* 277: 608–20, 1988.

Gizzi MS, Katz E, Schumer RA, and Movshon JA. Selectivity for orientation and direction of motion of single neurons in cat striate and extrastriate visual cortex. *J Neurophysiol* 63: 1529–1543, 1990.

Graf W, Simpson JI, and Leonard CS. Spatial organization of visual messages of the rabbit's cerebellar flocculus. II. Complex and simple spike responses of Purkinje cells. *J Neurophysiol* 60: 2091–2121, 1988.

Grasse KL and Cynader MS. Electrophysiology of medial terminal nucleus of accessory optic system in the cat. *J Neurophysiol* 48: 490–504, 1982.

Grasse KL and Cyander MS. The accessory optic system in frontal-eyed animals. In: *Vision and Visual Dysfunction. The Neuronal Basis of Visual Function*, edited by Leventhal A. New York: McMillan, 1990, p. 111–139.

Grasse KL, Cyander MS, and Douglas RM. Alterations in response properties in the lateral and dorsal terminal nuclei of the cat accessory optic system following visual cortex lesions. *Exp Brain Res* 55: 69–80, 1984.

Hoffmann KP and Distler C. Quantitative analysis of visual receptive fields of neurons in nucleus of the optic tract and dorsal terminal nucleus of the accessory optic tract in macaque monkey. *J Neurophysiol* 62: 416–428, 1989.

Hoffmann KP, Distler C, Erickson RG, and Mader W. Physiological and anatomical identification of the nucleus of the optic tract and dorsal terminal nucleus of the accessory optic tract in monkeys. *Exp Brain Res* 69: 635–644, 1988.

Hoffmann KP and Schoppmann A. Retinal input to direction selective cells in the nucleus tractus opticus of the cat. *Brain Res* 99: 359–366, 1975.

Hoffmann KP and Schoppmann A. A quantitative analysis of the direction-specific response of neurons in the cat's nucleus of the optic tract. *Exp Brain Res* 42: 146–157, 1981.

Holstege G and Collewijn H. The efferent connections of the nucleus of the optic tract and the superior colliculus in the rabbit. *J Comp Neurol* 209: 139–75, 1982.

Ibbotson MR, Mark RF, and Maddess TL. Spatio-temporal response properties of direction-selective neurons in the nucleus of the optic tract and the dorsal terminal nucleus of the wallaby, *Macropus eugenii. J Neurophysiol* 72: 2927–2943, 1994.

Ibbotson MR and Price NS. Spatio-temporal tuning of directional neurons in mammalian and avian pretectum: a comparison of physiological properties. *J Neurophysiol* 86: 2621–2624, 2001.

Ihaka R and Gentleman RR. A language for data analysis and graphics. *J Comp Graph Stats* 5: 299–314, 1996.

Ilg UJ. Slow eye movements. *Prog Neurobiology* 53: 293–329, 1997.

Ilg UJ and Hoffmann KP. Responses of neurons of the nucleus of the optic tract and the dorsal terminal nucleus of the accessory optic tract in the awake monkey. *Eur J Neurosci* 8: 92–105, 1996.

Itoh K. Efferent projections of the pretectum in the cat. *Exp Brain Res* 50: 89–105, 1977.

Kano M, Kano MS, Kusunoki M, and Maekawa K. Nature of optokinetic response and zonal organization of climbing fiber afferents in the vestibulocerebellum of the pigmented rabbit. II. The nodulus. *Exp Brain Res* 80: 238–51, 1990.

Karten HJ and Hodos W. *A Stereotaxic Atlas of the Brain of the Pigeon (Columba livia).* Baltimore, MD: Johns Hopkins Press, 1967.

Katte O and Hoffmann KP. Direction specific neurons in the pretectum of the frog (*Rana esculenta*). *J Comp Physiol* 140: 53–57, 1980.

Kawasaki T and Sato Y. Afferent projection from the dorsal nucleus of the raphe to the flocculus in cats. *Brain Res* 197: 496–502, 1980.

Klauer S, Sengpiel F, and Hoffmann KP. Visual response properties and afferents of nucleus of the optic tract in the ferret. *Exp Brain Res* 83: 178–189, 1990.

Kogo N, Fan TX, and Ariel M. Synaptic pharmacology in the turtle accessory optic system. *Exp Brain Res* 147: 464–472, 2002.

Kogo N, Rubio DM, and Ariel M. Direction tuning of individual retinal inputs to the turtle accessory optic system. *J Neurosci* 18: 2673–2684, 1998.

Kusunoki M, Kano M, Kano MS, and Maekawa K. Nature of optokinetic response and zonal organization of climbing fiber afferents in the vestibulocerebellum of the pigmented rabbit. I. The flocculus. *Exp Brain Res* 80: 225–237, 1990.

Langer TA, Fuchs F, Scudder CA, and Chubb MC. Afferents to the flocculus of the cerebellum in the rhesus macaque as revealed by retrograde transport of horseradish peroxidase. *J Comp Neurol* 235: 1–25, 1985.

Lau KL, Glover RG, Linkenhoker B, and Wylie DR. Topographical organization of inferior olive cells projecting to translation and rotation zones in the vestibulocerebellum of pigeons. *Neuroscience* 85: 605–614, 1998.

Levitt JB, Kiper DC, and Movshon JA. Receptive fields and functional architecture of macaque V2. *J Neurophysiol* 71: 2517–2542, 1994.

McKenna OC, and Wallman J. Identification of avian brain regions responsive to retinal slip using 2-deoxyglucose. *Brain Res* 210: 455–60, 1981.

McKenna OC, and Wallman J. Functional postnatal changes in avian brain regions responsive to retinal slip: a 2-deoxy-D-glucose study. *J Neurosci* 5: 330–342, 1985.

Morgan B and Frost BJ. Visual response properties of neurons in the nucleus of the basal optic root of pigeons. *Exp Brain Res* 42: 184–188, 1981.

Movshon JA, Adelson EH, Gizzi MS, and Newsome WT. The analysis of visual moving patterns. In: *Study Group on Pattern Recognition Mechanisms,* edited by Chagas C, Gattass R, Gross C. Vatican City, Italy: Pontificia Academia Scientiarum, 1985, p. 117–151.

Mustari MJ and Fuchs AF. Discharge patterns of neurons in the pretectal nucleus of the optic tract (NOT) in the behaving primate. *J Neurophysiol* 64: 77–90, 1990.

Nakayama K. Differential motion hyperacuity under conditions of common image motion. *Vision Res* 21: 1475–1482, 1981.

Papoulis A. *Probability and Statistics.* New York: Prentence-Hall International Editions, 1990.

Perrone JA and Thiele A. Speed skills: measuring the visual speed analyzing properties of primate MT neurons. *Nat Neurosci* 4: 526–531, 2001.

Price NS and Ibbotson MR. Direction-selective neurons in the optokinetic system with long-lasting after-responses. *J Neurophysiol* 88: 2224–2231, 2002.

Priebe NJ, Cassanello CR, and Lisberger SG. The neural representation of speed in macaque area MT/V5. *J Neurosci* 23: 5650–5661, 2003.

Reiner A and Karten HJ. A bisynaptic retinocerebellar pathway in the turtle. *Brain Res* 150: 163–169, 1978.

Robinson DA. Control of eye movements. In: *Handbook of Physiology. The Nervous System. Motor Control,* edited by Brooks VB. Bethesda, MD: *Am Physiol Soc* 1981, sect. 1, vol. II, p. 1275–1320.

Rosenberg AF and Ariel M. Visual-response properties of neurons in turtle basal optic nucleus in vitro. *J Neurophysiol* 63: 1033–1045, 1990.

Ruigrok TJ. Collateralization of climbing and mossy fibers projecting to the nodulus and flocculus of the rat cerebellum. *J Comp Neurol* 466: 278–98, 2003.

Sato Y, Kawasaki T, and Ikarashi K. Afferent projections from the brainstem to the three floccular zones in cats. II. Mossy fiber projections. *Brain Res* 272: 37–48, 1983.

Scannell JW, Sengpiel F, Tovee MJ, Benson PJ, Blakemore C, and Young MP. Visual motion processing in the anterior ectosylvian sulcus of the cat. *J Neurophysiol* 76: 895–907, 1996.

Simpson JI. The accessory optic system. *Rev Neurosci* 7: 13–41, 1984.

Simpson JI, Giolli RA, and Blanks RHI. The pretectal nuclear complex and the accessory optic system. *Rev Oculomot Res* 2: 335–364, 1988.

Simpson JI, Graf W, and Leonard C. The coordinate system of visual climbing fibres to the flocculus. In: *Progress in Oculomotor Research,* edited by Fuchs AF, and Becker W. Amsterdam: Elsevier/North Holland, 1981.

Simpson JI, Soodak RE, and Hess R. The accessory optic system and its relation to the vestibulocerebellum. *Prog Brain Res* 50: 715–724, 1979.

Soodak RE and Simpson JI. The accessory optic system of rabbit. I. Basic visual response properties. *J Neurophysiol* 60: 2055–2072, 1988.

Terasawa K, Otani K, and Yamada J. Descending pathways of the nucleus of the optic tract in the rat. *Brain Res* 173: 405–417, 1979.

Thach WT Jr. Somatosensory receptive fields of single units in cat cerebellar cortex. *J Neurophysiol* 30: 675–696, 1967.

Torigoe Y, Blanks RHI, and Precht W. Anatomical studies on the nucleus reticularis tegmenti pontis in the pigmented rat. I. Cytoarchitecture, topography, and cerebral cortical afferents. *J Comp Neurol* 243: 71–87, 1986a.

Torigoe Y, Blanks RHI, and Precht W. Anatomical studies on the nucleus reticularis tegmenti pontis in the pigmented rat. II. Subcortical afferents demonstrated by the retrograde transport of horseradish peroxidase. *J Comp Neurol* 243: 88–105, 1986b.

Venables WN and Ripley BD. *Modern Applied Statistics with S-Plus* (4th ed.). New York: Springer-Verlag, 2002.

Volchan E, Rocha-Miranda CE, Picanco-Diniz CW, Zinsmeisser B, Bernardes RF, and Franca JG. Visual response properties of pretectal units in the nucleus of the optic tract of the opossum. *Exp Brain Res* 78: 380–386, 1989.

Voogd J, Gerrits NM, and Ruigrok TJ. Organization of the vestibulocerebellum. *Ann NY Acad Sci* 781: 553–579, 1996.

Waespe W, Buttner U, and Henn V. Input-output activity of the primate flocculus during visual-vestibular interaction. *Exp Brain Res* 43: 337–348, 1981.

Weber JT. Pretectal complex and accessory optic system in alert monkeys. *Brain Behav Evol* 26: 117–140, 1985.

Westheimer G and McKee SP. Visual acuity in the presence of retinal-image motion. *J Opt Soc Am* 65: 847–50, 1975.

Winfield JA, Hendrickson A, and Kimm J. Anatomical evidence that the medial terminal nucleus of the accessory optic tract in mammals provides a visual mossy fiber input to the flocculus. *Brain Res* 151: 175–82, 1978.

Winship IR and Wylie DRW. Responses of neurons in the medial column of the inferior olive in pigeons to translational and rotational optic flowfields. *Exp Brain Res* 141: 63–78, 2001.

Winship IR and Wylie DRW. Zonal organization of the vestibulocerebellum in pigeons (*Columba livia*). I. Climbing fibre input to the flocculus. *J Comp Neurol* 456: 127–139, 2003.

Winterson BJ and Brauth SE. Direction-selective single units in the nucleus lentiformis mesencephali of the pigeon (*Columba livia*). *Exp Brain Res* 60: 215–226, 1985.

Wolf-Oberhollenzer F and Kirschfeld K. Motion sensitivity in the nucleus of the basal optic root of the pigeon. *J Neurophysiol* 71: 1559–1573, 1994.

Wylie DR. Projections from the nucleus of the basal optic root and nucleus lentiformis mesencephali to the inferior olive in pigeons (*Columba livia*). *J Comp Neurol* 429: 502–513, 2001.

Wylie DR, Bischof WF, and Frost BJ. Common reference frame for neural coding of translational and rotational optic flow. *Nature* 392: 278–282, 1998.

Wylie DR and Crowder NA. Spatio-temporal properties of fast and slow neurons in the pretectal nucleus lentiformis mesencephali in pigeons. *J Neurophysiol* 84: 2529–2540, 2000.

Wylie DR and Frost BJ. Visual response properties of neurons in the nucleus of the basal optic root of the pigeon: a quantitative analysis. *Exp Brain Res* 82: 327–336, 1990.

Wylie DR and Frost BJ. Responses of pigeon vestibulocerebellar neurons to optokinetic stimulation. II. The 3-dimensional reference frame of rotation neurons in the flocculus. *J Neurophysiol* 70: 2647–259, 1993.

Wylie DR and Frost BJ. The pigeon optokinetic system: visual input in extraocular muscle coordinates. *Vis Neurosci* 13: 945–953, 1996.

Wylie DR and Frost BJ. Responses of neurons in the nucleus of the basal optic root to translational and rotational flowfields. *J Neurophysiol* 81: 267–276, 1999.

Wylie DR, Kripalani T, and Frost BJ. Responses of pigeon vestibulocerebellar neurons to optokinetic stimulation. I. Functional organization of neurons discriminating between translational and rotational visual flow. *J Neurophysiol* 70: 2632–2646, 1993.

Wylie DR and Linkenhoker B. Mossy fibres from the nucleus of the basal optic root project to the vestibular and cerebellar nuclei in pigeons. *Neurosci Lett* 219: 83–86, 1996.

Wylie DR, Linkenhoker B, and Lau KL. Projections of the nucleus of the basal optic root in pigeons (*Columba livia*) revealed with biotinylated dextran amine. *J Comp Neurol* 384: 517–536, 1997.

Wylie DR, Winship IR, and Glover RG. Projections from the medial column of the inferior olive to different classes of rotation-sensitive Purkinje cells in the flocculus of pigeons. *Neurosci Lett* 268: 97–100, 1999.

Yakushin SB, Gizzi M, Reisine H, Raphan T, Buttner-Ennever J, and Cohen B. Functions of the nucleus of the optic tract (NOT). II. Control of ocular pursuit. *Exp Brain Res* 131: 433–447, 2000.

Zanker JM, Srinivasan MV, and Egelhaaf M. Speed tuning in elementary motion detectors of the correlation type. *Biol Cybern* 80: 109–116, 1999.